Spatial and spectral mode selection of heralded single photons from pulsed parametric down-conversion

S. Castelletto, I. P. Degiovanni, V. Schettini
IEN, Photometry Dept, Turin 10135, Italy
castelle@ien.it

A. Migdall
NIST, Optical Technology Division, Gaithersburg, MD 20899-8441, USA
migdall@nist.gov

Abstract: We describe an experiment in which photon pairs from a pulsed parametric down-conversion (PDC) source were coupled into single-mode fibers with heralding efficiencies as high as 70%. Heralding efficiency or mode preparation efficiency is defined as the probability of finding a photon in a fiber in a definite state, given the detection of its twin. Heralding efficiencies were obtained for a range of down-conversion beam-size configurations. Analysis of spatial and spectral mode selection, and their mutual correlation, provides a practical guide for engineering PDC-produced single photons in a definite mode and spectral emission band. The spectrum of the heralded photons were measured for each beam configuration, to determine the interplay between transverse momentum and spectral entanglement on the preparation efficiency.

OCIS codes: (190.4410) Nonlinear Optics; (270.0270) Quantum optics; (270.4180) Multiphoton process

References and links

1. D. N. Klyshko, *Photons and Nonlinear Optics*, (Gordon and Breach Science Publishers, 1988).
2. D. C. Burnham and D. L. Weinberg, "Observation of simultaneity in parametric production of optical photon pairs," Phys. Rev. Lett. **25**, 84-87 (1970).
3. C. K. Hong and L. Mandel, "Experimental realization of a localized one-photon state," Phys. Rev. Lett. **56**, 58-60 (1986).
4. A. I. Lvovsky, H. Hansen, T. Aichele, O. Benson, J. Mlynek, and S. Schiller, "Quantum State Reconstruction of the Single-Photon Fock State," Phys. Rev. Lett. **87**, 050402 (2001).
5. A. L. Migdall, S. Castelletto, I. P. Degiovanni, and M. L. Rastello, "Towards an intercomparison of a correlated photon based method to measure detector quantum efficiency," Appl. Opt. **41**, 2914-2922 (2002).
6. W. Tittel, J. Brendel, H. Zbinden and N. Gisin, "Quantum cryptography using entangled photons in energy-time bell states," Phys. Rev. Lett. **84**, 4737-40 (2000).
7. E. Knill, R. Laflamme, and G. J. Milburn, "A scheme for efficient quantum computation with linear optics," Nature **409**, 46-52 (2001).
8. M. Zukowski, A. Zeilinger, and H. Weinfurter,"Entangling photons radiated by independent pulsed sources," Ann. N.Y. Acad. Sci. **755**, 91 (1995). J. G. Rarity, "Interference of single photons from separate sources," Ann. N.Y. Acad. Sci. **755**, 624 (1995).
9. D. Bouwmeester, J. W. Pan, K. Mattle, M. Eibl, H. Weinfurter, and A. Zeilinger, "Experimental quantum teleportation," Nature **390**, 575-579 (1997).

#7518 - $15.00 USD
Received 3 June 2005; revised 9 August 2005; accepted 15 August 2005

10. S. Castelletto, I. P. Degiovanni, V. Schettini, M. Ware, and A. Migdall, "Measurement of coupling PDC photon source with single-mode and multi-mode optical fibers," in "*Quantum Communications and Quantum Imaging*," R. E. Meyers and Y. H. Shih, eds., SPIE Proc. **5551**, 60-72 (2004).
11. C. Kurtsiefer, M. Oberparlieter, and H. Weinfurter, "High-efficiency entangled photon pair collection in type-II parametric fluorescence," Phys. Rev. A **64**, 023802 (2001).
12. F. A. Bovino, P. Varisco, A. M. Colla, G. Castagnoli, G. Di Giuseppe, and A. V. Sergienko, "Effective fiber-coupling of entangled photons for quantum communication," Opt. Commun. **227**, 343-348 (2003).
13. C. H. Monken, P. H. Souto Ribeiro, and S. Padua, "Optimizing the photon pair collection efficiency: A step toward a loophole-free Bell's inequalities experiment," Phys. Rev. A **57**, R2267-R2269 (1998).
14. S. Castelletto, I. P. Degiovanni, M. Ware, and A. Migdall, "Coupling efficiencies in single photon on-demand sources," in "*Quantum Communications and Quantum Imaging*" R. E. Meyers and Y. H. Shih, eds., Proc. SPIE **5161**, 48-56 (2003).
15. S. Castelletto, I. P. Degiovanni, M. Ware, and A. Migdall, "On the measurement of two-photon single mode coupling efficiency in PDC photon sources," New J. of Phys. **6**, 87 (2004).
16. A. Dragan, "Efficient fiber coupling of down-conversion photon pairs," Phys. Rev. A **70**, 053814 (2004).
17. T. B. Pittmann, B. C. Jacobs, and J. D. Franson, "Heralding single photons from pulsed parametric down-conversion," Opt. Commun. **246**, 545-550 (2005).
18. D. Rosenberg, A. E. Lita, A. J. Miller, S. Nam, and R. E. Schwall, "Performance of photon-number resolving transition-edge sensors with integrated 1550 nm resonant cavities," IEEE Trans. Appl. Supercond. **15**, 575-578 (2005).
19. The fiber-coupled bandwidth in this Type-I PDC experiment is significantly larger than that of the Type-II PDC setup in reference [11].
20. Calculation according to the NIST program on the web page http://physics.nist.gov/Divisions/Div844/facilities/cprad/cprad.html
21. M. H. Rubin, "Transverse correlation in optical spontaneous parametric down-conversion," Phys. Rev. A **54**, 5349-5360 (1996).
22. We calibrated the detector efficiency by using a mulitmode fiber in the same configuration of coupling lenses used with the single mode fiber after testing that the CUT collected all the correlated photons.
23. N. Boeuf, D. Branning, I. Chaperot, E. Dauler, S. Guerin, G. Jaeger, A. Muller, and A. Migdall, "Calculating characteristics of noncollinear phase matching in uniaxial and biaxial crystals," Opt. Eng. **39**, 1016-1024 (2000).

1. Introduction

Parametric down-conversion (PDC) is known to produce a quantum state of light with a two-photon field description [1, 2]. However, if only one photon of the pair is measured, the source exhibits thermal statistical behavior. We can however reintroduce a certain degree of coherence; by measuring one of the photons, we prepare the other photon in a definite state [3, 4]. The prepared state will be pure only if we project the first PDC photon (called also the *heralding* photon) into a single mode. Recent studies target applications based on PDC, such as quantum metrology [5] and quantum information [6, 7] that work by preparing one photon by measuring its twin. To optimize this process, it is crucial to properly define and measure the efficiency of that preparation.

For certain quantum information processing applications [7], it is important to have the heralded photons in well-defined spectral and spatial modes. This is done by detecting one photon of a PDC pair in a certain spatial and spectral mode, and collecting the other photon in a correlated mode.

In recent years pulse-pumped PDC has been employed, followed by narrow-band spectral filtering for temporal mode definition [8, 9], and coupling the photons into single-mode fibers for spatial mode definition.

An important experimental parameter in such a single-photon source is the heralding efficiency, or the mode preparation efficiency, χ_P [10]. This is the efficiency of preparing a

#7518 - $15.00 USD Received 3 June 2005; revised 9 August 2005; accepted 15 August 2005

photon in the heralded channel in a definite spectral and spatial mode, by specific mode selection of the heralding or trigger arm. This is the probability to find the heralded photon in a specific state. It is evaluated by measuring the raw detection efficiency (coincidence / single counts), and correcting for detection losses in the *heralded* channel. In other words, given the biphoton state, the *heralding* channel projects the photon into a certain mode, by spectral and spatial selection which determines the final state of the *heralded* photon.

In this paper, we describe measurements of the heralding efficiency using a bulk-crystal Type-I PDC source pumped by pulses from a mode-locked laser. These measurements are related to earlier experimental work on coupling photon pairs from both continuous-wave (cw) [11] and pulsed [12] Type-II PDC bulk-crystal sources into single-mode fibers. Studies of PDC fiber-coupling issues can be found in references [10, 13, 14, 15, 16, 17]. A highlight of this paper is that we use an exact sinc function for the longitudinal phase-mismatch function allowing for better results in the long crystal case, as opposed to ref. [16] which uses a Gaussian approximation. In addition, this paper provides a formula for the absolute heralding efficiency and reports theoretical and experimental results comparable to the results reported in ref. [17]. We also note that if a photon-number resolving detector were used as the herald detector, the analysis presented here would apply to a heralded source of multi-photons as well. While the emission accuracy, and thus the ultimate N-photon heralding efficiency of a such a multi-photon source would require a high efficiency herald detector, high efficiency photon-number resolving detectors are now being reported [18].

2. Experimental setup

We used a fiber-coupling strategy based on the method described in [10]. An overview of the source is shown in Fig. 1. The idea is to prepare the *heralding* photon in a single spatial mode, and collect the *heralded* photon in a single spatial mode, where each mode is defined by a single-mode fiber. In both channels we define our single modes by backward propagating and imaging the single-mode fibers onto the PDC crystal as shown in Fig. 1. The goal is to match and overlap the single-mode beams in the crystal spatially, while considering the extra divergence due to the PDC phase-matching conditions over the wavelength range of interest. We prove that spatial overlap alone is not enough when we have pulsed pumping and that attention has to be paid to define spectrally the mode preparation efficiency. As expected, the mode selection is both spatial and spectral.

In our experiment, the PDC source was a 5 mm long $LiI0_3$ crystal pumped by frequency-doubled Ti-Sapphire laser pulses at a repetition rate of 76 MHz and a wavelength of 394.5 nm, with a duration of approximately 150 fs. The $LiI0_3$ crystal was oriented to produce photon pairs at 789 nm to 791 nm at an external cone angle of θ_0=3.4°, with a phase-matching internal angle of ϕ_o=44.15°.

Two small diametrically opposed regions of the emitted cone were coupled (at two different distances from the crystal, for cases (a) and (c) d_1=53 cm and d_2=38 cm, for case (b) the distances were reversed), into single-mode fibers using one of three optical configurations. The lens types (L_1 and L_2), locations, and resulting beam waists at the crystal are given in Table 1. The pump beam was focused at the crystal with a beam waist w_p of 260 μm. The output of the fibers were coupled onto the photon-counting detectors so as to underfill the active area so all light from the fiber could be detected. The detectors were commercially available Si avalanche photodiode modules with low dark count rates (≈50 Hz). The detector outputs were sent to a conventional coincidence

#7518 - $15.00 USD Received 3 June 2005; revised 9 August 2005; accepted 15 August 2005

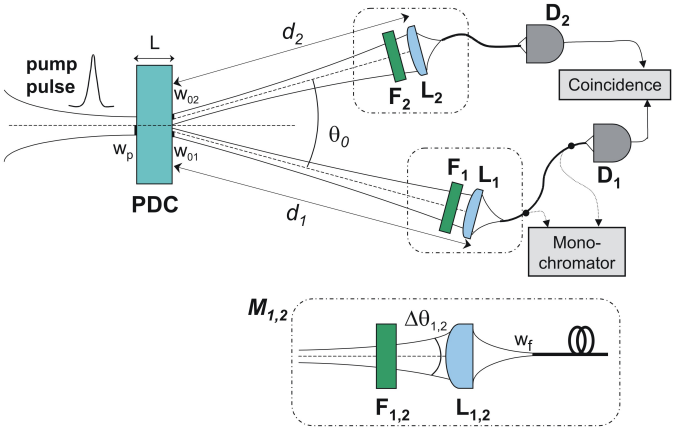

Fig. 1. Setup used to herald single-photons from pulsed parametric down-conversion (PDC). Filters $F_{1,2}$, either cut-off or interference and various lenses $L_{1,2}$ are used, according to Table I. Distances $d_{1,2}$ were chosen for practical reasons, and the direction 1 was the heralding channel except for lens configuration (b). A monochromator was inserted in the heralding channel fiber link to measure coincidence spectral distribution

circuit consisting of a time-to-amplitude converter and a single-channel-analyzer with a 4 ns coincidence window.

Table 1. Details of lens configurations for coupling fiber mode diameter of 4.2 μm, and M are magnifications.

lens configuration	L_1 @ d_1	$w_{0,1}$ (μm)	M_1	L_2 @ d_2	$w_{0,2}$ (μm)	M_2
(a)	Aspheric f=15.4 mm	70	33	μ obj., 20x, f=9 mm	85	40
(b)	μ obj., 20x, f=9 mm	85	40	μ obj., 20x, f=9 mm	127	61
(c)	Aspheric f=8 mm	137	65	Aspheric f=8 mm	97	47

3. Theoretical model

Even in the continuous wave (CW) case for type I phase matching, spectral mode selection is crucial [19]. This is easily understood from the phase matching curves for a gaussian pump beam and a long crystal. Figure 2 shows [20] the calculated output angle θ of the down-converted photons as a function of wavelength for approximately the experimental conditions of our setup. The thickness of the curve is due to the finite dimension transverse pump beam and the finite length crystal, when longitudinal mismatch is included. Calculating the PDC emission for a range of pump beam diameters and crystal lengths demonstrates that the fuzzyness or spread of the emission angle is due to these effects. For example, a larger pump beam waist gives reduced fuzzyness, while a longer crystal, where longitudinal phase-mismatch is present, decreases

#7518 - $15.00 USD
Received 3 June 2005; revised 9 August 2005; accepted 15 August 2005

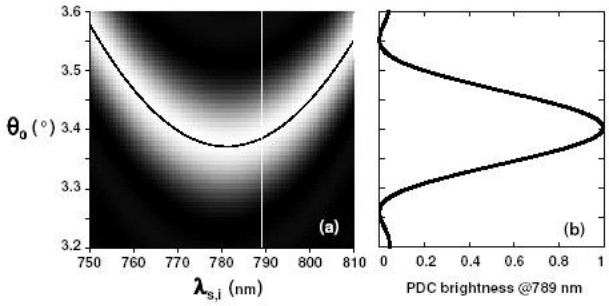

Fig. 2. (a) Calculated external angular PDC emission of $LiIO_3$ at a phase-matching angle of 44.15°, including the longitudinal mismatch and the pump transverse shape (gaussian with a 260 μm pump waist, crystal length L=5 mm). The black line is the central emission angle of PDC for the experimental condition, for a 395 nm CW pump beam, is superimposed. This calculation was done according to ref. [23], and the normalized phasematch function (perfect phasematch =1) is used. (b) Vertical slice of (a) at a wavelength of 789 nm.

the spread around the central emission angle.

Pulsed pumping is now introduced in the calculation [16]. In ref. [17] the effect of the pulsed pump beam on the PDC spectrum width is reported. Here, we use a theoretical approach to predict the spectral emission of the PDC coincidence and to optimize the spectral and spatial mode selection to maximize the mode preparation efficiency and we compare the theoretical prediction with the experimental results.

Our calculations, using the spatial mode preparation results obtained elsewhere [10, 15], decompose into two terms the spectral mode selection of the PDC represented in Fig. 2. We deduce the fiber spectral selection from the PDC angular central emission curve, while we account for the width due to the longitudinal wavevector mismatch to first order. The angular selection of a fiber-defined single mode beam, considered as a spatial filter, around the central emission angle of the PDC is obtained from $\theta_o(\lambda_{s,i})$(see Fig. 2). The geometric collection selected spectral width component at the full width half maximum (FWHM) by the fiber, $\Delta_{1,2}$, is approximately given by the FWHM angular collection $\Delta\theta_{1,2}$ of the fiber times the slope of the spectral/angular spread of the PDC, around the central wavelength λ_o, i.e.

$$\Delta_{1,2} = \Delta\theta_{1,2}[\frac{\partial\theta_o(\lambda)}{\partial\lambda}|_{\lambda_o}]^{-1}, \tag{1}$$

where $\Delta\theta_{1,2} = a\frac{\lambda}{\pi w_{o,1,2}}$, $a = \sqrt{2\ln(2)}$ is the conversion factor between the FWHM and the $1/e^2$ radius of the field profile and $w_{o,1,2}$ are the fiber waists at the crystal. Note that the lens clear apertures are greater than $\Delta\theta_{1,2}d_{1,2}$. The correlation between the spectral emission and the phase-mismatch in the longitudinal direction giving the fuzzyness for each wavelength, represented in Fig. 2(b), is instead partially included in the following theory, as it will be clear from Fig. 6.

We note [21] that the biphoton state can be written in terms of the classical pump $E_p(x,y,z,t)$ field and the signal and idler photons' negative frequency-portion of the

#7518 - $15.00 USD Received 3 June 2005; revised 9 August 2005; accepted 15 August 2005

electric field operators, $\widehat{E}_{s,i}^{(-)}(x,y,z,t)$, as

$$|\psi\rangle = \chi^{(2)} \int_{-\infty}^{\infty} \mathrm{d}t \int_V \mathrm{d}x\ \mathrm{d}y\ \mathrm{d}z\ E_p(x,y,z,t)\widehat{E}_s^{(-)}(x,y,z,t)\widehat{E}_i^{(-)}(x,y,z,t)|0_{\mathbf{k}_s,\omega_s}\rangle|0_{\mathbf{k}_i,\omega_i}\rangle. \quad (2)$$

Here we replace the classical pump field with its transversal and spectral Fourier transform, according to

$$E_p(x,y,z,t) = \int \mathrm{d}^3k_p \mathrm{d}\omega_p \widetilde{E}_{q_p}(\mathbf{q}_p)\widetilde{E}_{\nu_p}(\omega_p)e^{i\mathbf{k}_p\cdot\mathbf{r}-i\omega_p t}, \quad (3)$$

rewriting the two-photon state at the output surface of a PDC crystal oriented with its face perpendicular to the z-axis as obtained in ref. [15]

$$|\psi\rangle = \int \mathrm{d}^3k_\mathrm{s} \mathrm{d}\omega_\mathrm{s} \mathrm{d}^3k_\mathrm{i} \mathrm{d}\omega_\mathrm{i} \widetilde{A}_{12}(\mathbf{k}_\mathrm{s},\mathbf{k}_\mathrm{i},\omega_\mathrm{i},\omega_\mathrm{s})|1_{\mathbf{k}_\mathrm{s},\omega_\mathrm{s}}\rangle|1_{\mathbf{k}_\mathrm{i},\omega_\mathrm{i}}\rangle, \quad (4)$$

where

$$\begin{aligned}
\widetilde{A}_{12}(\mathbf{k}_\mathrm{s},\mathbf{k}_\mathrm{i},\omega_\mathrm{i},\omega_\mathrm{s}) \quad \propto \quad & \int \mathrm{d}^3k_\mathrm{p} \mathrm{d}\omega_\mathrm{p} \int_S \mathrm{d}x\mathrm{d}y \int_{-L}^{0} \mathrm{d}z\ \widetilde{E}_{\mathrm{q_p}}(\mathbf{q}_\mathrm{p})\widetilde{E}_{\nu_\mathrm{p}}(\omega_\mathrm{p})e^{i(\Delta k_x x+\Delta k_y y+\Delta k_z z)} \\
& \times\delta(\omega_\mathrm{s}+\omega_\mathrm{i}-\omega_\mathrm{p}) \\
& \times\delta\left[k_{p_z} - \sqrt{\left(\frac{n(\omega_p)\omega_p}{c}\right)^2 - \mathbf{q}_p^2}\right] \\
& \times\delta\left[k_{s_z} - \sqrt{\left(\frac{n(\omega_s)\omega_s}{c}\right)^2 - \mathbf{q}_s^2}\right] \\
& \times\delta\left[k_{i_z} - \sqrt{\left(\frac{n(\omega_i)\omega_i}{c}\right)^2 - \mathbf{q}_i^2}\right], \quad (5)
\end{aligned}$$

S is the cross sectional area of the crystal illuminated by the pump, and L is the length of the crystal. The subscripts s, i, p indicate the signal, idler, and pump. The pump beam propagates along the z axis. We evaluate $\Delta k_{x,y,z} = (\mathbf{k}_p - \mathbf{k}_s - \mathbf{k}_i)_{x,y,z}$, in terms of the pump, signal, and idler k-vectors. The longitudinal component of the pump k-vector is

$$k_{p_z} = \sqrt{\left(\frac{n(\omega_p)\omega_p}{c}\right)^2 - \mathbf{q}_p^2}, \quad (6)$$

where $\mathbf{q}_p$ is the transverse component of the pump k-vector and c is the speed of light. Analogous expressions give the signal and idler longitudinal components.

$\widetilde{E}_{\nu_p}(\omega_p) = \exp(-\frac{1}{8a^2}(\omega_p - \Omega_p)^2 T_p^2)$, is the pump pulse frequency distribution, where T_p is the width at FWHM and $\widetilde{E}_{q_p} = \exp(-\frac{w_p^2 q_p^2}{4})$ is the pump transverse wavevector distribution with w_p being the pump field waist. Both are assumed for simplicity to be Gaussian. We write the wavevector mismatch $\Delta k_{x,y,z}$ terms as

$$\begin{aligned}
\Delta k_x &= q_{p_x} - q_{s_x} - q_{i_x} \quad (7) \\
\Delta k_y &= q_{p_y} - q_{s_y} - q_{i_y} - \theta_i K_i - \theta_s K_s \\
\Delta k_z &= D_{pi}\nu_p + D_{is}\nu_s + (\mathscr{N}_p - \mathscr{N}_s)\frac{q_{p_y}}{K_p} + \theta_s q_{s_y} - \theta_i q_{i_y},
\end{aligned}$$

#7518 - $15.00 USD Received 3 June 2005; revised 9 August 2005; accepted 15 August 2005

where $\theta_{i,s}$ are the emission angles of the idler and signal photons, and $K_{i,s,p} = n_{i,s,p}(\Omega_{i,s,p},\phi)\Omega_{i,s,p}/c$ describe the directions of the central intensities of the wavevectors. The terms, $\mathscr{N}_p = \frac{\Omega_p}{c}\frac{\mathrm{d}n_p(\Omega_p,\phi)}{\mathrm{d}\phi}|_{\phi_o}$ and $\mathscr{N}_s = \frac{\Omega_s}{c}\frac{\mathrm{d}n_s(\Omega_s,\phi)}{\mathrm{d}\phi}|_{\phi_o}$ account for the effects of the refractive indexes of the pump and the signal due to the pump angular spread, which is responsible for a small deviation from the phase-matching angle ϕ_o. The other terms are defined as $D_{is} = -\frac{\mathrm{d}n_{\mathrm{i}}(\omega_{\mathrm{i}})\omega_{\mathrm{i}}/c}{\mathrm{d}\omega_{\mathrm{i}}}|_{\Omega_{\mathrm{i}}} + \frac{\mathrm{d}n_s(\omega_{\mathrm{s}},\phi)\omega_{\mathrm{s}}/c}{\mathrm{d}\omega_{\mathrm{s}}}|_{\Omega_{\mathrm{s}}}$, $D_{pi} = -\frac{\mathrm{d}n_{\mathrm{i}}(\omega_{\mathrm{i}})\omega_{\mathrm{i}}/c}{\mathrm{d}\omega_{\mathrm{i}}}|_{\Omega_{\mathrm{i}}} + \frac{\mathrm{d}n_{\mathrm{p}}(\omega_{\mathrm{p}},\phi)\omega_{\mathrm{p}}/c}{\mathrm{d}\omega_{\mathrm{p}}}|_{\Omega_{\mathrm{p}}}$ and $\nu_{i,s,p} = \omega_{\mathrm{i,s,p}} - \Omega_{\mathrm{i,s,p}}$ with $\nu_p = \nu_i + \nu_s$. Note that $\mathscr{N}_s = 0$ for Type I phase-matching. Assuming S infinite, we integrate over x and y, giving $\Delta k_x = \Delta k_y = 0$. To obtain the biphoton field in the transverse spatial and time variables, we take the Fourier transforms on the q and ν variables and integrate over z,

$$\begin{aligned} A_{12}(\rho_1,\rho_2,t,\tau) \quad \propto \quad & E_{\nu_p}(\frac{\tau - t + 2\tau D_{pi}/D_{is}}{2}) E_{q_p}(x_1, y_1 - \frac{\mathscr{N}_{p,s}\tau}{K_p D_{is}}) \\ & \delta(x_1 - x_2) \times \delta(y_1 - y_2 + \frac{\alpha_s \tau}{D_{is}}) \Pi_{D_{is}L}(\tau), \end{aligned} \tag{8}$$

where $\mathscr{N}_{p,s} = -\mathscr{N}_s + \mathscr{N}_p - K_p\theta_i$, $\alpha_s = \theta_i + \theta_s$, $\tau = t_1 - t_2$, $t = t_1 + t_2$ and $\Pi_{D_{is}L}(\tau) = 1$ for $0 \le \tau \le D_{is}L$ and 0 elsewhere. t_1 and t_2 are the times when the two photons are generated at the longitudinal positions z_1=z_2=0, at the crystal output surface.

To obtain Eq. (8) we made some approximations. First, we assumed that the pump, signal, and idler have narrow transverse angular distributions, so we can use the paraxial approximation. We also rewrite the longitudinal k-vector components by expanding the index of refraction $n_{p,s,i}(\omega_{p,s,i},\phi)$ around the central frequencies $(\Omega_{s,i})$, and around the phase-matching angle ϕ_o. This approximation holds only in cases where the considered field is an extraordinary wave (this of course depends on the type of phase-matching adopted, either type I or type II). In all cases we limited our calculation to the first perturbative order. We also assume small non-collinearity and small walk-off angles. $E_{\nu_p}(\frac{\tau - t + 2\tau D_{pi}/D_{is}}{2})$ is the time Fourier transform of the pump spectral distribution $\widetilde{E}_{\nu_p}(\nu_p)$ and $E_{q_p}(x_1, y_1 - \frac{\mathscr{N}_{s,p}\tau}{K_p D_{is}})$ is similarly the Fourier transform of pump transverse momentum distribution $\widetilde{E}_{q_p}$. To calculate the coincidence rates measured by two single mode fibers in the signal and idler arms, we assume first that the guided transverse spatial modes are Gaussian fields propagated back from the fibers through the lenses and crystal output surface, and are defined by

$$\varphi_j^*(x_j, y_j) = \sqrt{\frac{2}{\pi}} \frac{1}{w_{o,j}} \exp\left[-\frac{(x_j^2 + y_j^2)}{w_{o,j}^2} \right], \tag{9}$$

with $j = 1, 2$. The imaging optic L_j is arranged to place the collection beam waist, $w_{o,j}$ at the crystal. We work in the perfect imaging configuration where the gaussian field guided by a fiber is magnified by the lens and if $w_{f,j}$ is the fiber waist at the fiber exit tip, the beam waist at the crystal is $w_{o,j} = M_j w_{f,j}$.

The resulting time dependent biphoton field is calculated by integrating over the transverse spatial variables according to

$$A_{12}(t,\tau) = \int \mathrm{d}\rho_1 \mathrm{d}\rho_2 A_{12}(\rho_1,\rho_2,t,\tau) \varphi_1^*(\rho_1) \varphi_2^*(\rho_2). \tag{10}$$

Here we have to consider that either we spectrally select the PDC photons by an interference filter and/or by single spatial mode collection, acting also as a spectral

#7518 - $15.00 USD Received 3 June 2005; revised 9 August 2005; accepted 15 August 2005

filter. We eventually identify a single mode fiber as a spectral filter with a gaussian spectral distribution given by $\widetilde{I}_{\nu_{s,i}}(\nu_{s,i}) = e^{(-\frac{a^2}{\Delta_{1,2}^2}\nu_{s,i}^2)}$ with $\Delta_{1,2}$ being the FWHM of the spectral distribution. Therefore, by Fourier transforming the spectral filter distributions as $I_{\nu_s}(t-t'+\tau-\tau')$ and $I_{\nu_i}(t-t'-\tau+\tau')$, the coincidence rate is

$$C_{12} = \int \mathrm{d}t\mathrm{d}t'\mathrm{d}\tau\mathrm{d}\tau' A_{12}(t,\tau)A_{12}^*(t',\tau')\varphi_1^* I_{\nu_s}(t-t'+\tau-\tau')I_{\nu_i}(t-t'-\tau+\tau'). \tag{11}$$

Single channel event rates are calculated with only one fiber-defined spatial mode, i.e. first by calculating

$$A_{12}(t,\tau,\rho_2) = \int \mathrm{d}\rho_1 A_{12}(\rho_1,\rho_2,t,\tau)\varphi_1^*(\rho_1) \tag{12}$$

and then integrating over the spectral filter as

$$C_1 = \int \mathrm{d}\rho_2\mathrm{d}t\mathrm{d}t'\mathrm{d}\tau\mathrm{d}\tau' A_{12}(t,\tau,\rho_2)A_{12}^*(t',\tau',\rho_2)\varphi_1^* I_{\nu_s}(t-t'+\tau-\tau'). \tag{13}$$

The mode preparation efficiency is finally

$$\chi_{\mathrm{P}} = \frac{C_{12}}{C_1}. \tag{14}$$

For the case where arm 1 is the heralding channel with noncollinear degeneracy the result for type I PDC is

$$\chi_{\mathrm{P}} = \frac{4T_p\ w_{o,1}^2 w_{o,2}^2 w_p^2\ (w_{o,1}^2+w_p^2)\Delta_2}{(w_{o,2}^2 w_p^2 + w_{o,1}^2(w_{o,2}^2+w_p^2))^2\sqrt{8a^6+T_p^2(\Delta_1^2+\Delta_2^2)}}\frac{f(c_1,c_2)}{f(s_1,s_2)}, \tag{15}$$

where

$$f(p,q) = \frac{\int_0^1 \mathrm{d}x\ e^{-px^2+\frac{q^2x^2}{4p}}\,(\mathrm{Erf}[\frac{qx}{2\sqrt{p}}]-\mathrm{Erf}[\frac{-2p+qx}{2\sqrt{p}}])}{\sqrt{p}}. \tag{16}$$

The parameters are:

$$\begin{aligned}
c_1 &= \frac{L^2[w_{o,2}^2\alpha^2 + w_{o,1}^2(\alpha^2+K_p^2D_{pi}^2w_{o,2}^2(\Delta_1^2+\Delta_2^2))]}{K_p^2[w_{o,2}^2w_p^2+w_{o,1}^2(w_{o,2}^2+w_p^2)][a^2+a^{-2}\ T_p^2(\Delta_1^2+\Delta_2^2))]} \\
\alpha &= \sqrt{a^2\mathscr{N}_{s,p}^2 + [a^{-2}\mathscr{N}_{s,p}^2T_p^2 + K_p^2D_{pi}^2w_p^2(\Delta_1^2+\Delta_2^2)]} \\
c_2 &= \frac{2L^2D_{pi}^2(\Delta_1^2+\Delta_2^2)}{a^2+a^{-2}\ T_p^2(\Delta_1^2+\Delta_2^2)} \\
s_1 &= \frac{L^2[2\ a^{-2}\mathscr{N}_{s,p}^2T_p^2(w_{o,1}^2+2w_p^2) + K_p^2D_{pi}^2w_p^2(w_{o,1}^2+w_{o,2}^2)]}{2\ a^{-2}\ K_p^2T_p^2w_p^2(w_{o,1}^2+w_p^2)} \\
s_2 &= \frac{L^2[2\ a^{-2}\mathscr{N}_{s,p}^2T_p^2w_{o,1}^2 + K_p^2D_{pi}^2w_p^2(w_{o,1}^2+w_p^2)]}{2\ a^{-2}\ K_p^2T_p^2w_p^2(w_{o,1}^2+w_p^2)}.
\end{aligned} \tag{17}$$

The coincidence spectrum is determined by taking only the Fourier transform of the transverse spatial variables in Eq. (4), obtaining

$$\begin{aligned}
A_{12}(\rho_1,\rho_2,\nu_s,\nu_i) \quad \propto \quad & \widetilde{E}_{\nu_p}(\nu_s+\nu_i)E_{q_p}(x_1, y_1+(y_1-y_2)\frac{\mathscr{N}_{s,p}}{K_p\alpha_s})\times \\
& \exp[\frac{\mathrm{I}(y_1-y_2)(\nu_sD_{is}+(\nu_i+\nu_s)D_{pi})}{\alpha_s}]\ \delta(x_1-x_2)\Pi_{-L}(\frac{y_1-y_2}{\alpha_s}),
\end{aligned}$$

#7518 - $15.00 USD Received 3 June 2005; revised 9 August 2005; accepted 15 August 2005

where $\Pi_{-L}(\frac{y_1-y_2}{\alpha_s}) = 1$ for - $\alpha_s L \leq y_1 - y_2 \leq 0$ and 0 elsewhere.

Therefore the resulting frequency-dependent biphoton field is calculated by integrating over the transverse spatial variables according to

$$A_{12}(\nu_s, \nu_i) = \int \mathrm{d}\rho_1 \mathrm{d}\rho_2 A_{12}(\rho_1, \rho_2, \nu_s, \nu_i) \varphi_1^*(\rho_1) \varphi_2^*(\rho_2). \tag{18}$$

The coincidence spectrum for the degenerate case ($\Omega_s = \Omega_i$) is

$$C_{12}(\nu_i) = \int \mathrm{d}\nu_s |A_{12}(\nu_s, \nu_i)|^2 \widetilde{I}_{\nu_i}(\nu_i) \widetilde{I}_{\nu_s}(\nu_s) = \int \mathrm{d}\nu_s \mathscr{C}_{12}(\nu_i, \nu_s). \tag{19}$$

(Note that the pump spectral width due to its pulsed nature explicitly adds to the width of this coincidence spectrum.) We explicitly write $\mathscr{C}_{12}(\nu_i, \nu_s)$ as

$$\begin{aligned} \mathscr{C}_{12}(\nu_i, \nu_s) \quad \propto \quad & |\widetilde{E}_{\nu_p}[(\nu_s + \nu_i)(1 + \frac{8\, a^2 \zeta^2}{T_p^2})^{1/2}]|^2 \widetilde{I}_{\nu_i}(\nu_i) \widetilde{I}_{\nu_s}(\nu_s) \times \\ & |\mathrm{Erf}[\gamma + \zeta(\nu_s + \nu_i)] - \mathrm{Erf}[\zeta(\nu_s + \nu_i)]|^2, \end{aligned} \tag{20}$$

where

$$\begin{aligned} \zeta &= -\frac{K_p D_{pi} \sqrt{w_{o,2}^2 w_p^2 + w_{o,1}^2 (w_{o,2}^2 + w_p^2)}}{2 \mathscr{N}_{s,p} \sqrt{(w_{o,1}^2 + w_{o,2}^2)}}, \\ \gamma &= -L \sqrt{\frac{w_p^2 + w_{o,2}^2}{w_p^2 w_{o,2}^2 + w_{o,1}^2 (w_p^2 + w_{o,2}^2)}} \frac{\mathscr{N}_{s,p}}{K_p}. \end{aligned}$$

From Eq. (20) we deduce that the interplay between the spectral components $\nu_{i,s}$ and the transverse parameters $w_{o,p}$ is quantified by ζ, contained in the Erf terms, which is relevant to both the pump pulse envelope and the pump transverse distribution. Note that while for w_p large, the term $\widetilde{E}_{\nu_p}[(\nu_s + \nu_i)(1 + \frac{8\, a^2 \zeta^2}{T_p^2})^{1/2}]$ contributes to a widened coincidence spectrum, the Erf terms instead reduce the overall coincidence spectrum. In our experimental setup for pump waists bigger than 300 μm, the overall effect is a very slight dependence of the coincidence spectrum on the pump waist. However, when we sharply focus the pump beam waist to on the order of 30 μm, we expect a broader coincidence spectrum. This means that for small pump waist, the correlation is strong and the spectral and transverse components are not separable. The correlation could be better estimated if we included second order terms in the calculation, which were neglected here to a allow a tractable analytical solution.

4. Experimental results

We now analyze the coincidence spectrum for the specific optical setup used. A Gaussian beam analysis yields FWHM angular spreads of $\Delta\theta_{1,2}$ for the photon field according to the lens configurations in Table II.

From Fig. 2 and Eq. (1), it can be seen that the acceptance angles $\Delta_{1,2}$ allow down-converted photons with a raw bandwidth at the narrowest of Δ_2=21 nm to be coupled into our fibers.

We used a spectral filter F_1 centered at 789.3 nm with FWHM of 5 nm in the heralding channel (trigger) to obtain the best heralding efficiency. A cut off filter F_2 was used to

#7518 - $15.00 USD Received 3 June 2005; revised 9 August 2005; accepted 15 August 2005

Table 2. Angular spread collection and resulting χ_P's for each lens configuration

lens configuration	$w_{0,1}(\mu m)$	$\Delta\theta_1$ (°)	Δ_1 (nm)	$w_{0,2}(\mu m)$	$\Delta\theta_2$ (°)	Δ_2 (nm)	χ_P(theory) (%)	χ_P(expt.) (%)
(a)	70	0.24	56	85	0.19	46	92	55
(b)	85	0.19	46	127	0.13	30	77	61
(c)	137	0.12	29	97	0.17	40	86	70

reduce the background light in the other arm, which is here referred to as channel under test (CUT). A monochromator with 1 nm resolution was used for the coincidence spectral scan. F_1 reduced the bandwidth of the accepted trigger photons along with the bandwidth of the heralded photons. In this way, the choice of F_1 can be used to tailor the spectral properties of the heralded photons. Figure 3(a,b,c) shows the effects of restricting the accepted herald photon bandwidth to 5 nm (centered at 789 nm) versus the case where only the raw bandwidths (namely the herald and CUT bandwidths) are selected by the two fibers are used, for 3 different spectral widths given by different $L_{1,2}$ lens configurations. It is clear that, even in the absence of the interference filter, the overall coincidence bandwidth (heralded bandwidth) is reduced with respect to the single fiber selection spectral bandwidths, $\Delta_{1,2}$, and this is the signature that even in this case we have an entanglement between transverse and spectral components. For different configurations (a,b,c) we obtained measured heralded bandwidth ranging from 18 nm to 34 nm. With the 5 nm interference filter inserted, the final bandwidth is about 4 nm. The theoretical predictions match quite well with the experimental results.

These results show a narrow coincidence spectral bandwidth profile with respect to the estimated single channel bandwidth selection ($\Delta_{1,2}$), because the heralding channel bandwidth and the correlation dominate. Moreover to restrict the coincidence bandwidth, a narrow filter on the heralding arm is necessary. This means that a spatial mode defined by the single mode fiber contains a wider spectral mode.

To determine the difference between the spatial mode and the spectral mode selection operated by the single mode fibers, we measured the mode preparation efficiency and the single counts of the heralded channel versus an iris aperture at the collecting lens, with the configuration two f=8 mm (configuration (c)). We observed that the heralding efficiency, and the single CUT counts level off for almost the same iris aperture, correspondent to a measured waist of the mode at the lens of roughly 1.1 mm, which is in agreement with a gaussian mode of 2.1 μm waist at the fiber tip back propagated through a f=8 mm lens, in a perfect imaging configuration.

We made a coincidence spectral scan for various fixed iris apertures. The result is plotted in Fig. 4.

From the measured spectral scan, we see that the spectral width is independent of iris diameter down to at least 1 mm, which is to be expected as the "spectral mode waist" was estimated to be 0.7 mm ($1/\sqrt{2}$ of the spatial waist). In other words, in this case the fiber is just a spatial filter, providing an intensity profile selection. However to obtain the highest efficiency we must match the spatial modes, which are spatially wider than the spectral modes selected by the fiber. In contrast, spectral modes do not have to be matched. This is more evident in the pulsed case than in the CW case. In fact, the use of matched filters (F_1 and F_2) in pulsed PDC will cause an undesirable loss of heralded photons. The CUT arm bandwidth needs to be significantly wider than that of the trigger-photon filter F_1.

Figure 5 shows that narrow trigger bandwidth and wide CUT channel, yield the

#7518 - $15.00 USD Received 3 June 2005; revised 9 August 2005; accepted 15 August 2005

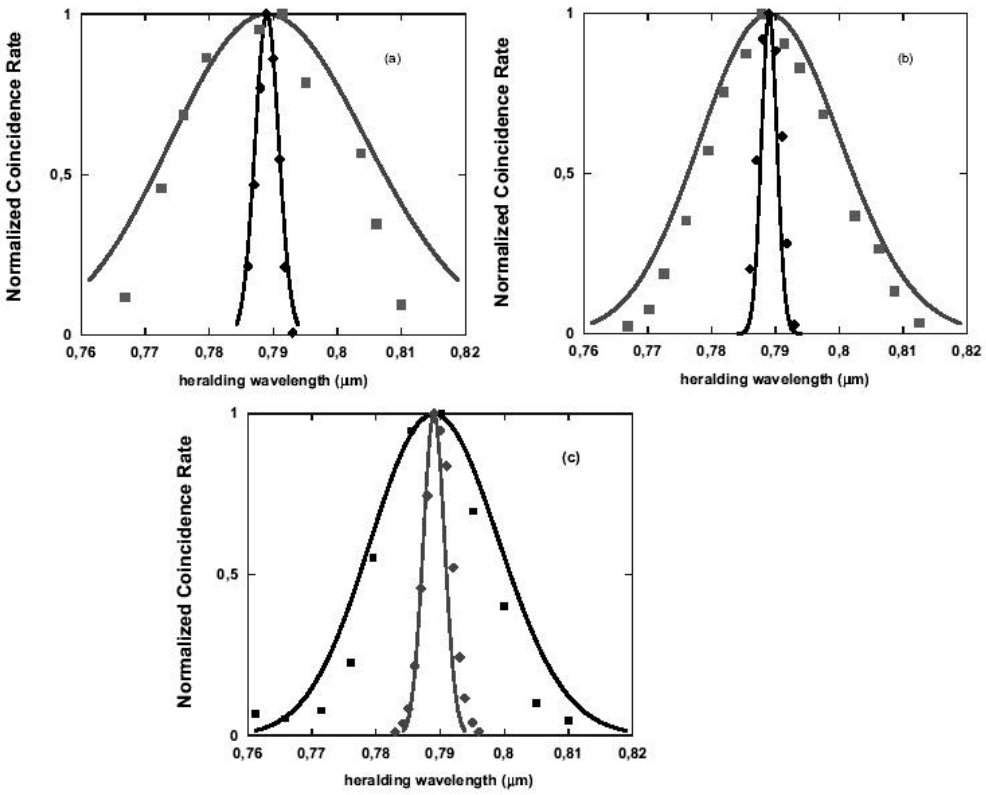

Fig. 3. Spectral scan of the normalized coincidence rates performed with a monochromator in the heralding fiber path. Solid lines are theoretical curves of Eq. (19). Lens configurations (a), (b) and (c). The narrower scans were taken with a 5 nm FWHM interference filter on the heralding arm.

highest mode preparation efficiency. This simulation assumes the perfect spatial mode matching condition, $w_{o,1} = w_{o,2} = w_o = Mw_f$ and $w_p >> w_o$, with equal heralding and heralded arms. The efficiency is higher for smaller lens magnification, for long focal lengths and/or short lens/crystal distances.

The experimental mode preparation efficiency was obtained by measuring the conditional detection efficiency of heralded photons, and then correcting for the losses in the heralded-photon arm. The conditional detection efficiency χ_{D} was simply defined as the coincidence counting rate, R_c, divided by the trigger photon detection rate, R_1.

Loss in the CUT-photon analysis path of Fig. 1 was due to a calibrated detector D_2 quantum efficiency of η=53.7% at 790 nm [22], a measured F_2 transmittance of 91% for the cut-off filter, and a measured transmittance of 96% for the nonlinear crystal at 790 nm. In addition, we estimate 4% reflectance loss upon exiting fiber and connecting to the detectors coupling lens, and an additional 2% loss due to the four anti-reflection-coated surfaces of the lens L_2. The total of these losses, along with the measured conditional detection efficiency of $\chi_{\mathrm{D}} = 31\%$, implies a mode preparation efficiency of $\chi_p = 70\%$. Our setup for practical reasons did not allow for exact spatial mode matching of the heralding and heralded modes (in fact, d_1 and d_2 were different). This is one of the

#7518 - $15.00 USD Received 3 June 2005; revised 9 August 2005; accepted 15 August 2005

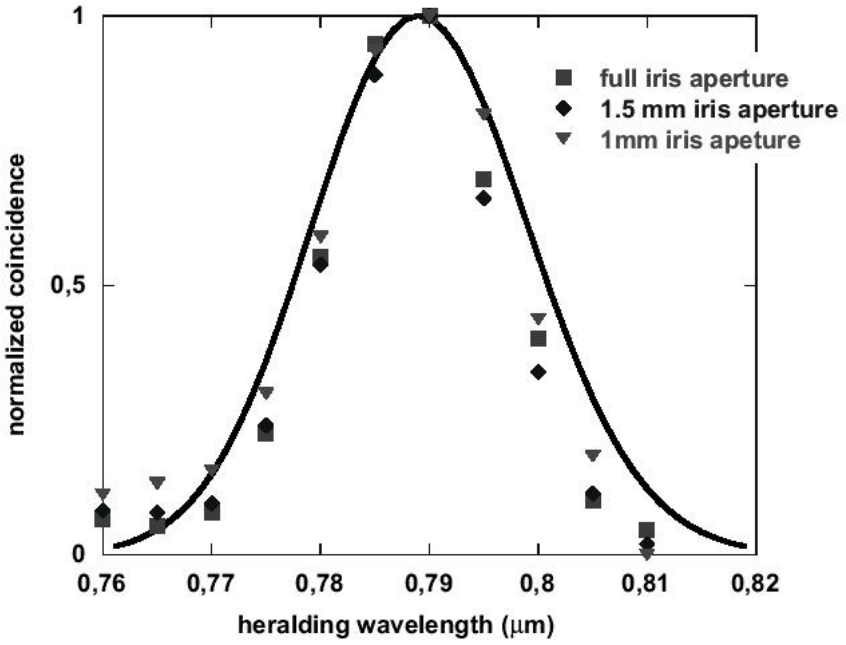

Fig. 4. Spectral scan coincidence for various iris diameters on the CUT arm. Data (squares for the full aperture, diamonds at 1.5 mm iris diameter, and down triangles for 1 mm iris diameter) are compared to the theoretical prediction.

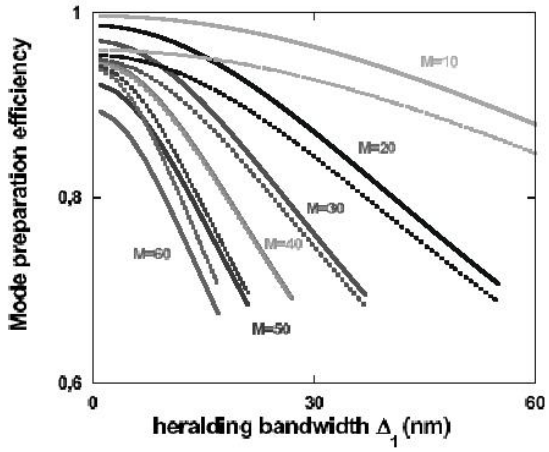

Fig. 5. Theoretical prediction of the mode preparation efficiency versus the trigger bandwidth for various lens magnifications. Lens magnification is given by $M_{1,2} = \frac{d_{1,2}-f_{1,2}}{f_{1,2}}$. Calculations are done for $w_{o,1} = w_{o,2} = w_o = Mw_f$ and a crystal 5 mm long. Solid lines are for for fixed $w_p = 260\ \mu$m and dotted line for $w_p = 3\ w_o$.

#7518 - $15.00 USD
Received 3 June 2005; revised 9 August 2005; accepted 15 August 2005

reason we could not reach the highest efficiency. The highest value was obtained with the (c) lens configuration. Here the predicted value is 86%. We obtained different maximum values for mode preparation efficiency in the other lens configurations. For lens configurations (a) and (b) we obtained 55%, and 61%, respectively, where the predicted values were 90% and 77%, respectively. The (b) configuration gives lower efficiency where the heralding channel had the shorter distance, yielding a narrower heralded channel bandwidth. Though the (a) configuration should yield the highest efficiency (lower magnification, longer focal length), in practice the NA of the single lens was only 0.15, which was inadequate to collect the entire spatial mode guided by the fiber. According to our prediction, a lower magnification in a perfect spatial mode matching configuration could yield the highest mode preparation efficiency for any defined trigger spectral selection. As an explanation of the 20% discrepancy between the predicted and measured single mode preparation efficiency, we show in Fig. (6) a comparison between the PDC intensity transverse angular profile of the heralded arm from a heralding single direction and single wavelength point, calculated as in [23] (a) and using the approximation of this paper (b). Because of the non-perfect longitudinal phase-matching and of the finite transverse pump profile, a single direction in the heralding arm corresponds to an area of correlated photons. As is visible, the transverse profile in a correct calculation is broader and equal in both dimensions, while in our approximation, it appears narrower in the y direction. This is because we retain only the first order in the series for the longitudinal mismatch, the remaining transverse contribution is only in the y direction as it is clearly evident from Eq. (7).

5. Conclusion

In this paper we analyzed theoretically and experimentally strategies to maximize the heralding efficiency of a PDC pulsed single-photon source, considering spatial and spectral mode selection. We provided a theoretical estimate of the heralding efficiency and of the coincidence spectrum for a pulsed type I PDC source, giving a practical method to tailor heralded photons in a defined spectral and spatial mode. This theoretical analysis of spatial and spectral mode coupling would also apply to a heralded source of N photons, if a photon-number resolving detector were used as the herald detector. That application would clearly require a herald detector with high efficiency, otherwise the accuracy of the N-photon emission would be poor. This would be a particularly critical problem for large N. Although we have not provided a specific efficiency analysis for this application, as such detectors advance, this application may warrant further attention.

This work was supported in part by ARDA, ARO, and DARPA/QUIST.

#7518 - $15.00 USD Received 3 June 2005; revised 9 August 2005; accepted 15 August 2005

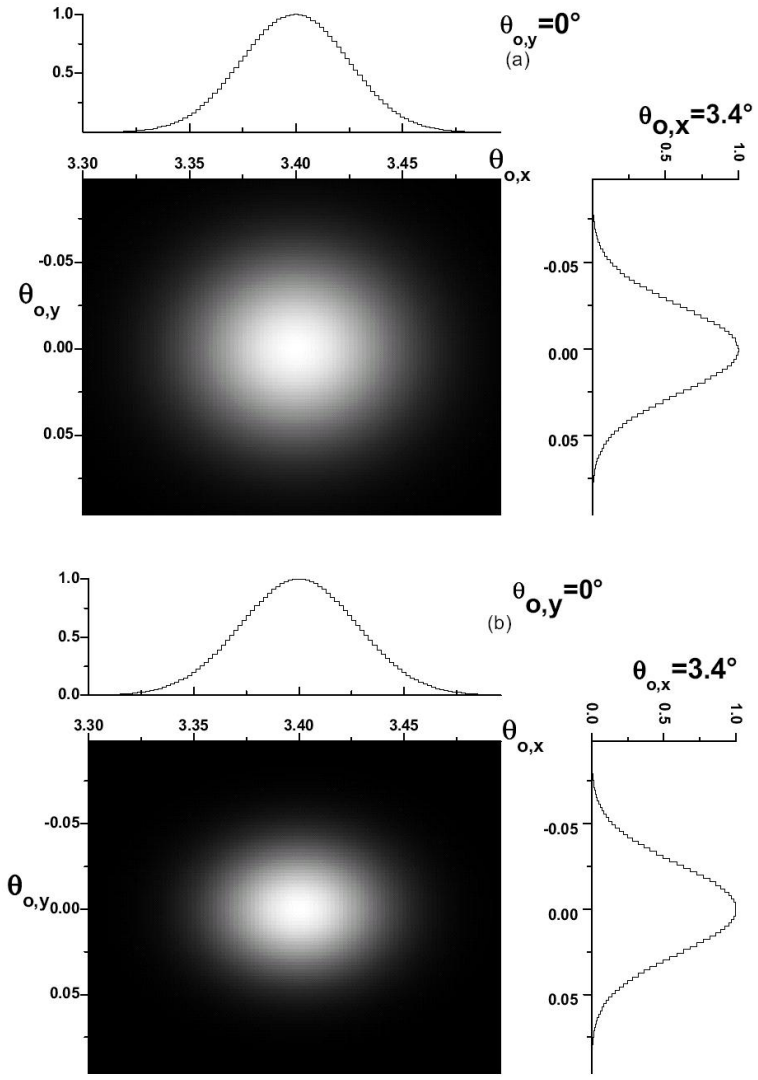

Fig. 6. Transverse intensity profile of the heralded PDC photon by a fixed heralding single direction and wavelength, calculated exactly (a) and with the present approximation (b).

#7518 - $15.00 USD
Received 3 June 2005; revised 9 August 2005; accepted 15 August 2005